International Journal of Engineering and Science Invention (IJESI)
ISSN (Online): 2319-6734, ISSN (Print): 2319-6726
www.ijesi.org ||Volume 13 Issue 8 August 2024 || PP 12-22

Catalytic Performance of Base Metal Addition into Mn/CeO_2 Catalyst for Low Temperature Oxidative Coupling of Methane

Ellen Gustiasih Maulidanti, Kenji Asami
(Faculty of Environmental Engineering, The University of Kitakyushu, Japan)

ABSTRACT: *The addition of Mn into a CeO_2-based catalyst has been proven to promote C_2 products at low temperature OCM reactions. However, the addition of Mn results in additional lattice oxygen, which contributes to CO_2 production. The addition of another metal is expected to increase the amount of surface electrophilic oxygen by changing the lattice oxygen reactivity of the 33 wt% of manganese/CeO_2 (33Mn/Ce) catalyst, resulting in improved oxygen evolution via active metal addition. A series of 33MnX/Ce catalysts with various X metals were developed. The 33 wt% of manganese and 15 wt% of calcium over CeO_2 catalyst (33Mn15Ca/Ce) has the highest catalytic activity at 450 °C. The catalysts were evaluated using XRD, Raman, N_2 adsorption-desorption, and XPS analysis, which revealed that the addition of Ca promotes the formation of Mn^{3+} cation. However, the number of oxygen vacancies has decreased, but the amount of surface electrophilic oxygen has increased. 33Mn15Ca/Ce catalyst performs better in oxygen-rich conditions and has a longer contact time.*

KEYWORDS – *Base metal, cerium oxide, low temperature, manganese oxide, oxidative coupling of methane*

Date of Submission: 03-08-2024 Date of Acceptance: 14-08-2024

I. Introduction

Methane (CH_4), which makes up over 16% of worldwide emissions, is the second most prevalent anthropogenic greenhouse gas after carbon dioxide (CO_2). It traps heat in the atmosphere more than 28 times more effectively than CO_2 [1]. Achieving a notable reduction in CH_4 would have a swift and substantial impact on the potential for atmospheric warming because it is a potent greenhouse gas and has a shorter half-life than CO_2.

The industrial sector employs CH_4 to generate greater heat as a power source. However, this process emits carbon as a byproduct of combustion, which is CO_2. On the other hand, CH_4 is used as a raw material in the steam reforming process to produce H_2 and syngas. Despite its multistep process, it requires a significant expenditure. Another approach to using CH_4 is to partially oxidize it into ethane (C_2H_6), which is subsequently dehydrogenated into ethylene (C_2H_4). This process is known as oxidative coupling of methane (OCM).

To accommodate CH4 activation, OCM typically requires a high reaction temperature. The Mn_2O_3-Na_2WO_4/SiO_2 catalyst has been investigated because of its good catalytic activity at 900 °C, which includes 20% CH_4 conversion and 60% C_2 selectivity [2]. This high reaction temperature (over 800 °C) is required to overcome the high energy of breaking the C-H bond in CH_4 molecules. On the other hand, a high reaction temperature can cause uncontrollable deep oxidation, resulting in CO_2, which should be avoided. A high reaction temperature facilitates a gas phase interaction between oxygen and CH_4 to produce CO_2 and H_2O, reducing C_2 output. Consequently, to manage the risk of deep oxidation, OCM must be considered at low temperature conditions. At low reaction temperatures, methane will be driven to react with active oxygen species on the catalyst surface rather than gas phase oxygen to form methyl radical. This low temperature condition also prevents the methyl radicals from desorbing to the gas phase, where they will couple to produce ethane. Thus, an appropriate catalyst is required to enable the production and coupling of methyl radicals on the catalyst surface.

Cerium oxide (CeO_2) has been proposed as a promising material due to its high oxygen storage capacity (OSC). OSC is the ability to store and release oxygen, resulting in oxygen vacancy condition that is useful for the generation of active oxygen species. This active oxygen species is essential for C_2 formation. Three active oxygen species involved in the OCM process are Superoxide (O_2^-), peroxide (O_2^{2-}), and lattice oxygen (O^{2-}). Both O_2^- and O_2^{2-} are selective in C_2H_6 generation, which is advantageous, whereas O^{2-} is selective in CO_2 generation. To get the requisite C_2 yield, CeO_2 must be combined with another metal oxide capable of increasing the amount of active oxygen species, particularly O_2^- and O_2^{2-}.

In our prior study, we mixed CeO_2 with nickel (Ni), cobalt (Co), and iron (Fe). The combination of Fe and CeO_2 has been reported as the only catalyst capable of producing 0.7% C_2H_6 yield and 17% CH_4 conversion at 500 °C. Unfortunately, the addition of Fe to CeO_2 did not stimulate the production of C_2H_4 [3]. To address this issue, we substituted Mn for Fe, which is renowned as a catalytic oxidation catalyst due to its high reducibility, ability to store and release oxygen, and ability to initiate oxidation at a low light-off temperature. Various amounts of Mn were examined, and we discovered that adding more than 33% of Mn to CeO_2 is hazardous due to its

increased formation of MnO_2 crystals, which reduces C_2 yield. At 450 ^oC the 33Mn/Ce catalyst converts 28% of methane, yielding 1.4% and 0.6% of C_2H_6 and C_2H_4, respectively. However, the presence of MnO_2 on the catalyst surface was shown to lower C_2H_6 yield. It could lead to O^{2-} formation, which is involved in C_2H_6 yield reduction [19]. To suppress the generation of O^{2-}, another addition of metal oxide to the 33Mn/Ce catalyst is being examined. We intend to increase the amount of superoxide and peroxide by modifying the lattice oxygen reactivity of the Mn/CeO_2 catalyst to improve oxygen evolution.

In this study, 33% of manganese and X% of base metal /CeO_2 (33MnX/Ce) samples with different X base metals such as calcium (Ca), lanthanum (La), lithium (Li), and zirconium (Zr), were synthesized by the impregnation method. 33Mn10Ca/Ce displays the best reaction performance at low reaction temperature with 31% of CH_4 conversion, 1.4% and 0.8% of C_2H_6 and C_2H_4 yield at 450 ^oC, respectively. Furthermore, the amount of Ca was examined to observe the influence of Ca rate on catalytic activity. It was found that 15% of Ca addition to 33Mn/Ce catalyst increased the catalytic activity to 2% and 0.9% of C_2H_6 and C_2H_4 yield at 450 ^oC, respectively. Various operating conditions are also studied, including the effect of temperature, CH_4/O_2 ratio, and contact time on the catalytic activity. The catalysts were characterized by XRD, Raman Spectroscopy, N_2 sorption, and XPS, which provide an understanding of the influence of metal addition towards the number of active oxygen species on the catalyst surface that are important for catalytic activity.

II. Materials And Methods

2.1 Catalyst preparation

The impregnation approach was used to generate a variety of 33MnX/Ce catalysts using various X metals (X = Ca, La, Li, and Zr). The Mn precursor was obtained from $Mn(NO_3)_2.6H_2O$ (99.99%, Wako Chemicals), with 33wt% of the Mn going into CeO_2 (nanoparticle CeO2, 99.99%, Sigma Aldrich). Ca, La, Li, and Zr precursors were produced from $Ca(NO_3)_2.4H_2O$ (99.99% Wako Chemicals), $La(NO_3)_3.6H_2O$ (99.99% Merck), $HCO_2Li.H_2O$ (98% Alfa Aesar), and $ZrO(NO_3)_2.2H_2O$ (99.99% Wako Chemicals). $Mn(NO_3)_2.6H_2O$ was dissolved in 20 mL of deionized water and agitated for 30 minutes at room temperature (Solution A), resulting in 33wt% Mn towards CeO_2. The specific catalyst synthesis of 33Mn/Ce catalyst is reported in our previous work [19]. On the other hand, each designated metal precursor was measured to 10wt% Ca, La, Li, or Zr towards CeO_2 and directly dissolved into 20 mL of deionized water, which was then agitated for 30 minutes at room temperature (solution B).

Solution A and Solution B were then combined and agitated for an additional 30 minutes at room temperature. The mixture and measured powder CeO_2 were then combined in a vacuum evaporator at 60 °C for 2 hours with steady stirring. The viscous solution was then vacuum-dried for 12 hours at 110 °C. The dried product was subsequently calcined at 400 ^oC for 12 hours, obtaining 33Mn10Ca/Ce, 33Mn10La/Ce, 33Mn10Li/Ce, and 33Mn10Zr/Ce, respectively. Those catalytic activities were then evaluated, and more catalyst synthesis at various metal rates was conducted.

In the following experiment, the 33MnX/Ce catalyst which had the best catalytic activity was further observed to see the influence of metal rate towards the catalytic activity. A series of 33MnX/Ce catalysts with varying X rates were synthesized using the impregnation method. The X precursor with X rate of 5wt%, 10wt%, 15wt%, 20wt%, and 30wt% toward CeO2 was measured and promptly dissolved into 20 mL of deionized water, then agitated for 30 minutes at room temperature. The rest of the synthesis process was identical to the prior one. The catalyst was crushed in a mortar until powdery and then formed with a hydraulic pressing machine. The pressed catalyst was crushed and sieved to acquire particle sizes of 355-450 µm.

2.2 Catalyst evaluation

The catalytic performance test was conducted in a fixed bed quartz tube reactor with an inner diameter of 4 mm at 1 atm. 0.06 gr of each catalyst with a distinct metal addition was placed on a glass wool bed in the center of the reactor and heated to 450°C. The reaction temperature was observed by placing a thermocouple into the reactor and contacting the catalyst bed. The feed has a total flow rate of 83 mL per minute. The feed contains 55 mL min^{-1} of CH_4 and 28 mL min-1 of oxygen. Subsequently, the catalyst with the best metal addition was investigated at different metal rates to determine the optimal metal rate, observe its influence on catalytic activity, and study the catalyst characteristic compared to the 33Mn/Ce catalyst. After determining the optimal rate, an experiment at various temperatures was undertaken. The reactor was heated from 350 ^oC with a temperature gap of 50 ^oC to 750 ^oC. In addition, the CH_4/O_2 ratio was investigated in 2, 3, and 4 using balanced argon (Ar). The final experiment investigated the effect of contact time using varied W/F values of 0.15, 0.3, and 0.6. To get steady state kinetic data, all sample injections were taken 5 minutes after stabilization at each temperature. Components in the reactant and product were evaluated using two on-line gas chromatographs: a Shimadzu GC-8A with TCD for O_2, CO, CO_2, and CH_4, and a Shimadzu GC-2014 with FID for CH_4, C_2H_6, and C_2H_4.

2.3 Catalytic characterization

The best metal doped catalyst at its optimal metal rate was characterized, along with the 33Mn/Ce catalyst for comparison purposes. The bulk phase composition of all catalysts was studied by X-ray diffraction on the Rigaku XPD-DSC with Ni-filtered Cu-Kα radiation. N_2 adsorption-desorption analysis at 77 K on the BELSORP-mini II revealed the porous characteristics. The specific surface area and pore size distributions were determined using the Brunauer-Emmet-Teller (BET) and Barret-Joyner-Halenda (BJH) techniques, respectively. The catalyst surface properties were investigated using Raman spectroscopy on an XploRA PLUS Horiba Raman spectrometer equipped with a 520 nm laser excitation source. To examine catalyst surface composition, X-ray Photoelectron Spectroscopy (XPS) tests were performed on an ALAT system employing a single MgKα X-ray source running at 200 W and 10 kV of voltage. The spectra were collected at room temperature using an ultrahigh vacuum. The binding energies were calibrated using the C 1s peak of graphite (284.6 eV) as a benchmark.

III. Results and Discussion

3.1 Catalytic performance of 33MnX/Ce catalyst

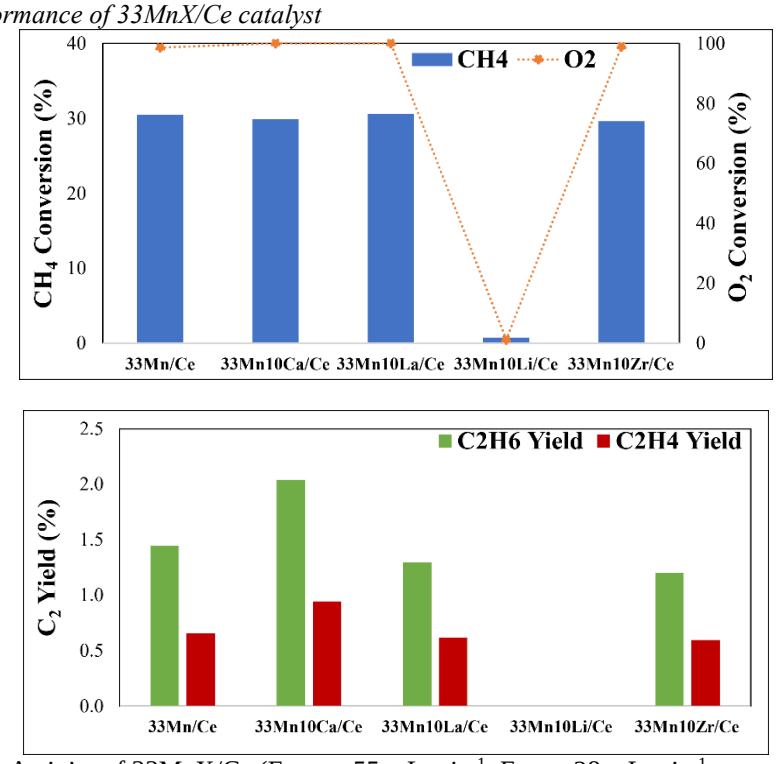

Fig.1. Catalytic Activity of 33MnX/Ce ($F_{(CH4)}$ = 55 mL min^{-1}; $F_{(O2)}$ = 28 mL min^{-1}, temperature = 450 ºC, catalyst weight = 60 mg, W/F = 0.3 g h mol^{-1})

Fig. 1 depicts the catalytic performance of the catalysts for the OCM process. The addition of Ca, La, and Zr showed no significant effect on catalytic activity when compared to the 33Mn/Ce catalyst. At 450 ºC, 33Mn10Ca/Ce, 33Mn10La/Ce, and 33Mn10Zr/Ce have already exhibited substantial activity in the reaction, with around 30% CH_4 conversion and 100% O_2 conversion, indicating that using Ca, La, and Zr may keep the 33Mn/Ce catalyst active at low temperatures. 33Mn10Li/Ce has the least activity of any catalyst. Almost no O_2 was converted, resulting in extremely low CH_4 conversion. 33Mn10Ca/Ce clearly surpasses all other catalysts, achieving 30% CH_4 conversion, 2.04% C_2H_6 yield, and 0.94% C_2H_4 yield at 450 ºC. On the other hand, the 33Mn/Ce catalyst is more active than the 33Mn10La/Ce and 33Mn10Zr/Ce catalysts, showing that the addition of Ca not only retains the potential to convert methane but also boosts the formation of C_2 products over the 33Mn/Ce catalyst at low reaction temperatures. This phenomenon could occur because the acid-base nucleophilic of Mn-O is attacked by Ca^{2+} cation, which decreases the Mn reactivity to bond with O, allowing O-O direct coupling. This O-O bonding may produce either O_2^- or O_2^{2-}, which is favorable in C_2 synthesis [4].

Because Ca addition produces the best results when compared to other metals, 33Mn10Ca/Ce was tested at different Ca rates to see how Ca rates affect catalytic activity, as shown in Fig. 2. As Ca is added to the catalyst at a rate of 15wt%, CH_4 conversion remains constant but the amount of C_2 produced gradually increases. However, when Ca was added up to 20%, catalyst activity decreased significantly, and no converted CH_4 was detected. This shows that adding more above 15wt% is detrimental to the OCM catalyst activity. It shows that too much Ca inhibits oxygen adsorption into the catalyst surface, prohibiting the formation of active oxygen species like O_2^-,

O_2^{2-}, and even O^{2-} on the catalyst surface, resulting in the inability to activate CH_4. As a result, 33Mn15Ca/Ce was the most effective catalyst in this study, with 31% of CH_4 Conversion, 2% of C_2H_6 yield and 1% of C_2H_4 yield.

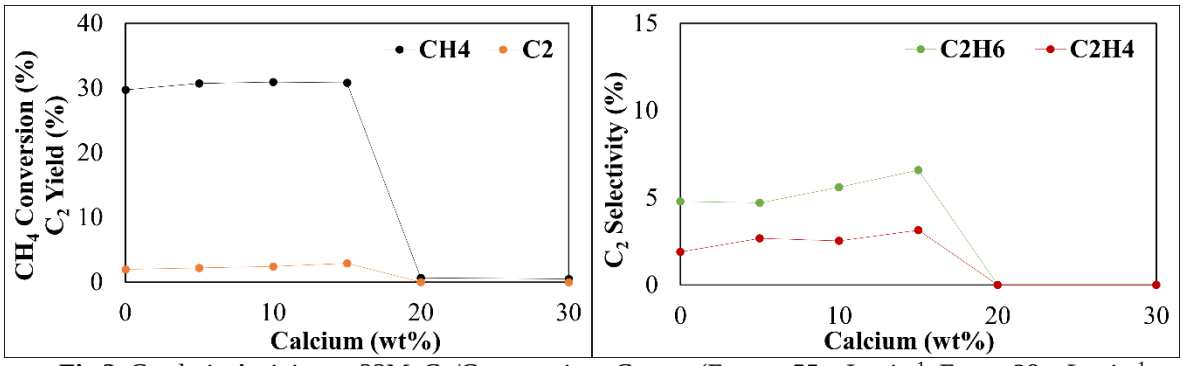

Fig.2. Catalytic Activity on 33MnCa/Ce on various Ca rate ($F_{(CH4)}$ = 55 mL min^{-1}; $F_{(O2)}$ = 28 mL min^{-1}, temperature = 450 °C, catalyst weight = 60 mg, W/F = 0.3 g h mol^{-1})

3.2. Characterization of catalysts

3.2. 1. X-Ray Diffraction

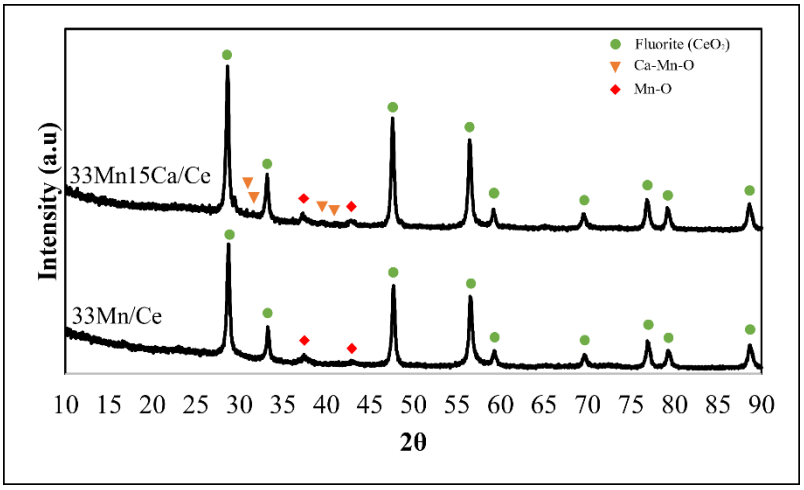

Fig.3. XRD patterns of 33Mn15Ca/Ce and 33Mn/Ce catalyst

XRD analysis was used to determine the crystal phases of 33Mn15Ca/Ce and 33Mn/Ce catalysts. Fig. 3 shows that both catalysts have substantial diffraction peaks at 28.7, 33.2, 47.5, 56.5, 59.3, 69.4, 76.9, 79.4, and 88.6°. The peaks are assigned to the cubic fluorite structure of CeO_2, indicating that the original structure of CeO_2 was preserved. Furthermore, both catalysts demonstrated additional XRD peaks at 37.4 and 42.6°, which contributed to the diffraction peak of Mn-O compounds, which is similar to MnO_2 [5][6]. Furthermore, certain peaks were found over the 33Mn15Ca/Ce catalyst at 31.4, 39.3, and 40.7°, indicating the presence of Ca-Mn-O molecules similar to $CaMn_3O_6$ perovskite [7].

3.2. 2. Raman Spectroscopy

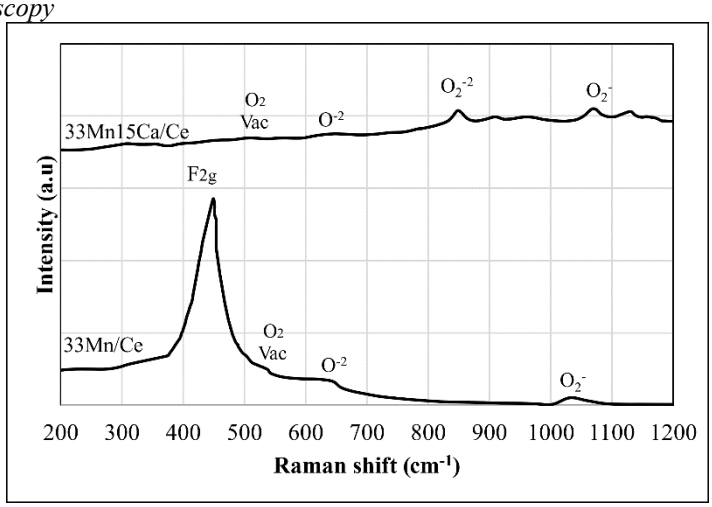

Fig.4. Raman spectroscopy of 33Mn15Ca/Ce and 33Mn/Ce catalysts

Raman spectroscopy was used to investigate the changes in catalyst structure, as shown in Fig. 4. An intense peak at 449 cm^{-1} is ascribed to the F_{2g} vibration of the fluorite-type lattice CeO_2 over the 33Mn/Ce catalyst [8]. It can be thought of as a symmetric breathing mode of oxygen atoms around Ce^{4+} ions in octahedral CeO_8 [9]. Furthermore, three peaks appeared at 543, 644, and 1050 cm^{-1}, corresponding to O_2 vacancies, O^{2-} anion, and O_2^- anion, respectively.

On the other hand, the peak representing the F_{2g} mode cubic fluorite structure of CeO_2 disappeared over the 33Mn15Ca/Ce catalyst. The absence in the F_{2g} mode could be due to a change in the lattice constant. The addition of Mn and Ca to the Ce lattice caused flaws, resulting in a Raman peak shift that is asymmetrical and broadened. In this example, the over-broadening peak of the F_{2g} mode occurred because of the excess Ca addition to CeO_2, which altered the M O vibration frequency to the Ce structure [10]. As a result, an extra peak at 854 cm^{-1} developed, corresponding to the O_2^{2-} anion, which was created as charge compensation defects caused by the insertion of other metal cations into the crystal lattice of CeO_2. What makes it intriguing is that the addition of Ca not only produces O_2^{2-}, but also broadens the O_2 vacancies and O^{2-}peaks at 568 and 647 cm^{-1}, respectively. Furthermore, the peak at 1075 cm^{-1}, which is ascribed to O_2^-, has a little higher peak intensity than the 33Mn/Ce catalyst. As a result, it is possible to conclude that although the 33Mn15Ca/Ce catalyst has fewer oxygen vacancies than 33Mn/Ce, it produces less O^{2-}, more O_2^-, and generates O_2^{2-}, which is beneficial for the OCM reaction.

3.2. 3. N_2 adsorption-desorption measurement

Table 1

Physicochemical properties of the freshly calcined catalysts measured by N_2 sorption.

Catalysts	BET surface area (m^2g^{-1})	Pore volume (cm^3g^{-1})	Pore size (nm)
33Mn/Ce	52.5	0.24	17.28
33Mn15Ca/Ce	14.5	0.07	19.45

N_2 adsorption-desorption measurements were done to determine the specific surface area and the pore size distribution of the catalyst, as shown in Fig. 5. 33Mn15Ca/Ce exhibits type I isotherm, indicating the existence of a microporous structure, whereas 33Mn/Ce exhibits type V isotherm, indicating the presence of a small degree of mesoporous structure. According to the BJH pore distribution analysis, 33Mn15Ca/Ce has an average pore size of less than 20 nm, indicating a micropore structure. The 33Mn/15Ce catalyst likewise has a micropore structure with a tiny percentage of mesopore size. Table 1 shows the BET surface area for each catalyst. Ca addition to 33Mn/Ce catalyst reduces surface area and pore volume.

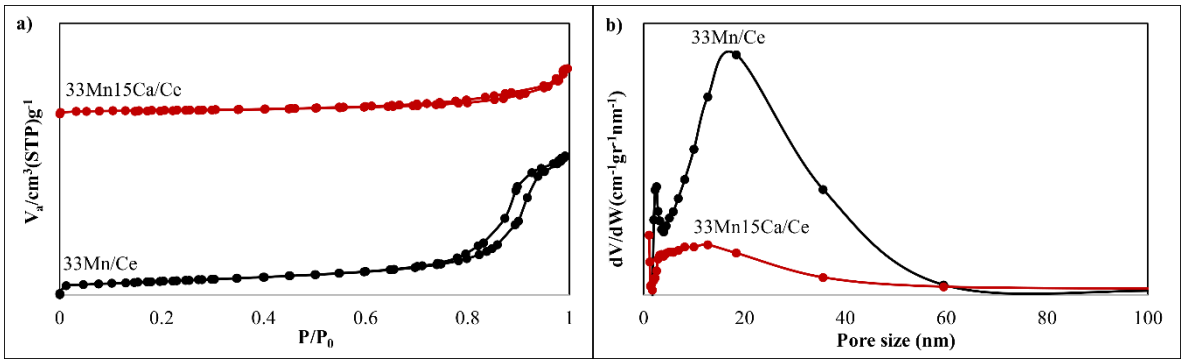

Fig.5. a) N_2 sorption measurement of 33Mn15Ca/Ce and 33Mn/Ce catalysts b) pore distribution of 33Mn15Ca/Ce and 33Mn/Ce catalysts

3.2. 4. X-ray photoelectron spectroscopy (XPS)

The surface composition of the catalysts was further examined using the XPS technique. Fig. 6(a) and 6(b) show the overall XPS spectra of the 33Mn/Ce and 33Mn15Ca/Ce catalysts, respectively. There was no Ca 2p peak observed over the 33Mn/Ce catalyst, whereas a Ca 2p peak was detected over the 33Mn15Ca/Ce catalyst. Figure 6(c) shows the XPS Ca spectra of the 33Mn15Ca/Ce catalyst, which has doublet Ca $2p_{3/2}$ and Ca $2p_{1/2}$ peaks. The binding energy corresponds to the divalent state Ca^{2+} cations, which vary from 345 to 355 eV [11].

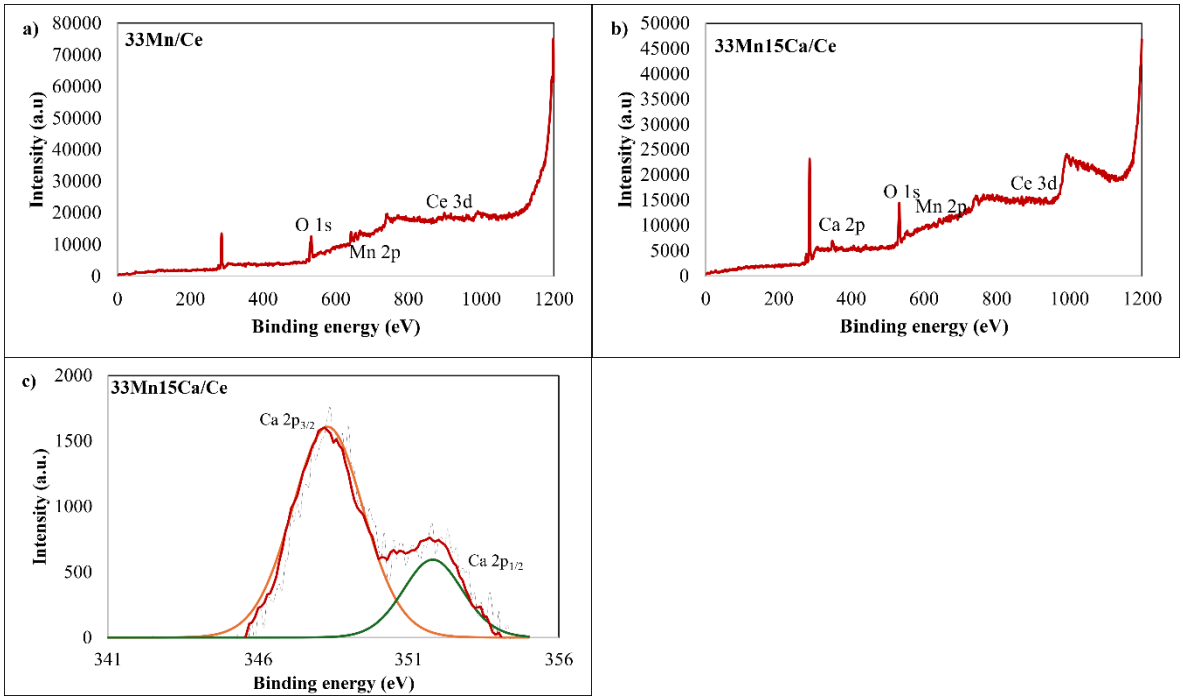

Fig.6. XPS spectra a) 33Mn15Ca/Ce b) 33Mn/Ce c) Ca2p peaks for 33Mn15Ca/Ce

According to the literature on ceria-based catalysts, oxygen vacancy is directly related to surface Ce^{3+} concentration [12]. Fig. 7 depicts the distribution of surface Ce cations. Because the valence state of ceria may be easily converted from trivalent to tetravalent, both Ce^{3+} and Ce^{4+} cations could be detected on the catalyst surface. As a result, the surface concentration of Ce^{3+} on the catalyst is calculated computationally using the summation of integrated peak areas of Ce^{3+} and Ce^{4+} XPS peaks. Both catalysts had doublet Ce $3d_{5/2}$ and Ce $3d_{3/2}$ peaks, with many peaks corresponding to the state Ce^{3+} and Ce^{4+} cation binding energies [13]. As shown in Table 2, 33Mn/Ce has a higher Ce^{3+} concentration than 33Mn15Ca/Ce.

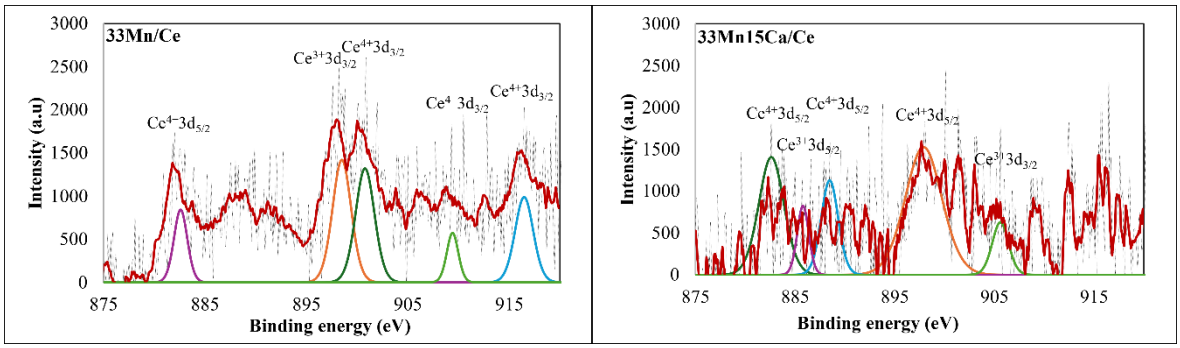

Fig.7. XPS spectra of Ce3d peaks for 33Mn15Ca/Ce and 33Mn/Ce catalysts

To obtain more direct information regarding surface oxygen properties, the O 1s spectra of the catalysts are examined in detail in Fig. 8. The original spectra reveal two overlapping O 1s peaks for each catalyst. The peak at 529 eV is reliably assigned to O^{2-}. Furthermore, another peak at 532 eV was thought to be surface carbonate, which inert to OCM reaction [14][15]. On all catalysts, an O_2^-peak between 535 and 539 eV is found. Furthermore, 33Mn15Ca/Ce shows an extra peak at 530 eV which corresponds to O_2^{2-}. According to related literature, O_2^- and O_2^{2-} sites are active and selective for the OCM reaction, but the O^{2-} site may be more devoted to deep oxidation of the hydrocarbon reactants and products. Table 2 quantifies the $(O_2^-+O_2^{2-})/O^{2-}$ ratio for each catalyst. This ratio appears to be consistent with the catalytic performance at 450 ºC, as depicted in Fig. 9. As a result, the addition of Ca to the 33Mn/Ce catalyst increases the amount of surface electrophilic oxygen (O_2^- and O_2^{2-}).

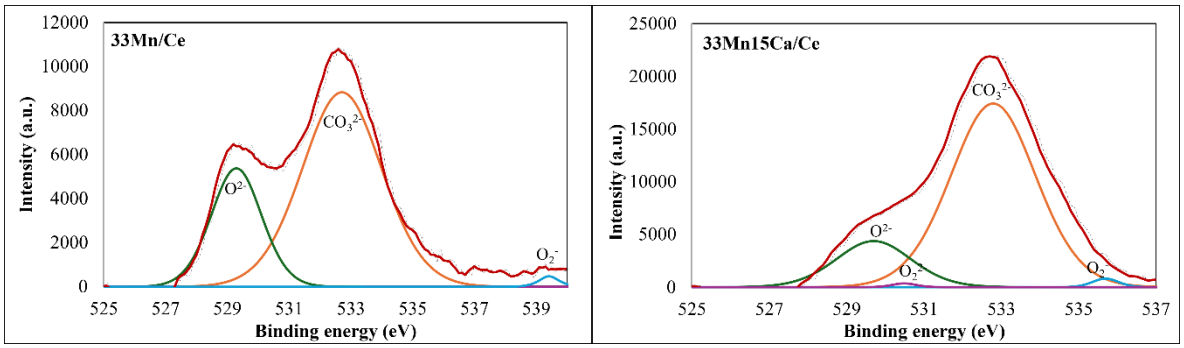

Fig.8. XPS spectra of O1s peaks for 33Mn15Ca/Ce and 33Mn/Ce catalysts

Table 2

The XPS quantification results of the catalysts.

Catalysts	Ce^{3+} (%)	Mn^{3+} (%)	O1s B.E (eV)/ relative amount (%)				$\frac{O_2^- + O_2^{2-}}{O^{2-}}$
			O_2^-	CO_3^{2-}	O_2^{2-}	O^{2-}	
33Mn/Ce	30.3	50.2	539.3/0.2	532.7/71.5	-	529.3/27.5	0.04
33Mn15Ca/Ce	14.8	70.7	535.1/2	532.8/78.9	530.5/0.5	529.7/17.5	0.14

Fig. 10 shows the doublet peaks Mn $2p_{3/2}$ and Mn $2p_{½}$ on both catalysts. On the 33Mn/Ce catalyst, the Mn $2p_{3}/2$ peaks can be classified into three peaks: Mn^{3+} (641.9 eV), Mn^{4+} (645 eV), and Mn^{2+} (647.9 eV) [16]. The Mn $2p_{1/2}$ peaks can be separated into two peaks: Mn^{4+} (653.3 eV) and Mn^{2+} (657.2 eV) [16]. The Mn $2p_{3/2}$ peaks for 33Mn15Ca/Ce catalyst, on the other hand, can be divided into two peaks: Mn^{3+} (642.2 eV) and Mn^{2+} (648.1) [16][17]. The Mn $2p_{1/2}$ peaks can be separated into two peaks: Mn^{4+} (654.1 eV) and Mn^{2+} (656.3 eV) [16].

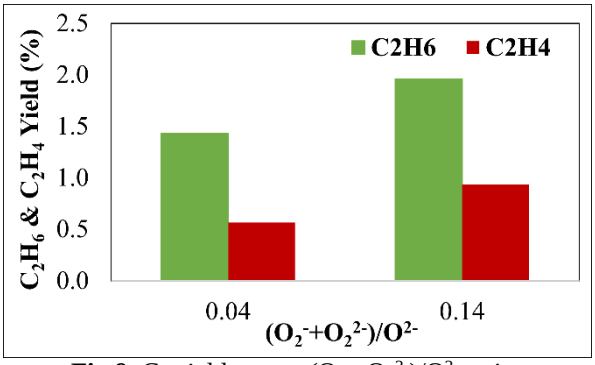

Fig.9. C_2 yield versus $(O_2^-+O_2^{2-})/O^{2-}$ ratios

Generally, Mn with a high oxidation state can improve oxidation performance at low temperatures [6]. Asami [18] found that the presence of Mn^{3+} cations on the catalyst surface correlates with methyl radical coupling capacity. As indicated in Table 2, adding Ca raised the number of Mn^{3+} cations by up to 70%. This demonstrates that the presence of Ca ions not only promotes the amount of surface electrophilic oxygen but also promotes the amount of Mn^{3+} cations, both of which are beneficial for the OCM process.

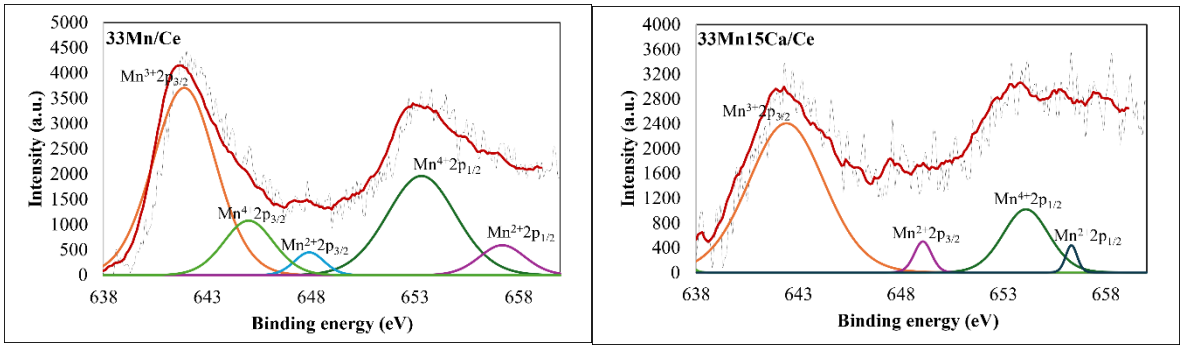

Fig.10. XPS spectra of Mn2p peaks for 33Mn15Ca/Ce and 33Mn/Ce catalysts

3.3. Catalytic performance in various operating conditions

3.3. 1. Reaction temperature

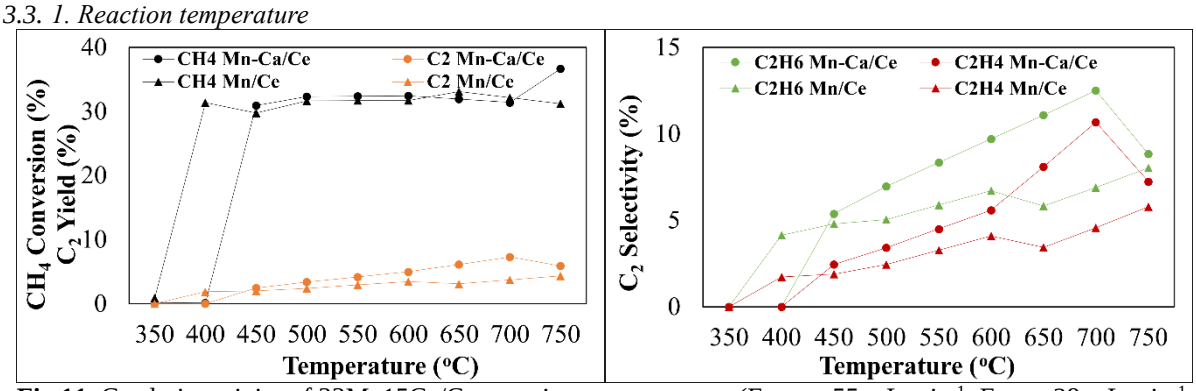

Fig.11. Catalytic activity of 33Mn15Ca/Ce at various temperatures ($F_{(CH4)}$ = 55 mL min^{-1}; $F_{(O2)}$ = 28 mL min^{-1}, temperature = 350-750 ºC (temperature gap of 50 ºC), catalyst weight = 60 mg, W/F = 0.3 g h mol^{-1})

To have a better knowledge of the 33Mn15Ca catalyst, additional observations on temperature influence were conducted. In addition to 33Mn15Ca/Ce, 33Mn/Ce was tested at 350ºC to 750ºC for comparison. As indicated in Fig. 11, neither 33Mn/Ce nor 33Mn15Ca/Ce could convert CH_4 at 350 ºC. Furthermore, the 33Mn/Ce catalyst outperforms the 33Mn15Ca/Ce catalyst at 400 ºC. As previously stated, 33Mn/Ce catalyst contains more Ce^{3+} cations than 33Mn15Ca/Ce. The number of Ce^{3+} cations on the catalyst corresponds to the number of oxygen vacancies. The oxygen vacancy can store and transform O_2 into active oxygen species. This oxygen species is significant in the low-temperature oxidation of CH_4. Furthermore, the Mn XPS spectra in Fig. 10 shows that 33Mn/Ce contains more Mn^{4+} cations on its surface. As previously stated, Mn^{4+} cations in the 33Mn/Ce catalyst improve oxidation performance at low temperatures. This is consistent with the XRD investigation, which

revealed the existence of MnO_2, which is the highest valence state of Mn. As a result, the 33Mn/Ce catalyst could carry out the reaction at a lower temperature than the 33Mn15Ca/Ce catalyst, which is 400 ºC.

However, when the temperature is raised to 450 ºC, the performance of the 33Mn15Ca/Ce catalyst improves significantly beyond the 33Mn/Ce catalytic activity. It is worth noting that the inclusion of Ca not only diminishes Mn reactivity toward O_2 but also alters the light-off temperature of the OCM process. The XRD investigation revealed an extra peak, which is thought to represent the formation of $CaMn_3O_6$ perovskite. $CaMn_3O_6$ could have formed because the Ca^{2+} cation attacked the acid nucleophilic of high valence Mn species, the H^+ from the Mn-O-H bond, because the surface hydroxyl Mn-O-H of high valence Mn tends to liberate H^+ [20]. As a result, the Mn species transitions to a lower valence state, $CaMn^3O^6$, where the Mn valence state is about 3,3. The O_2 is most likely to adsorb on the Mn^{3+} [20], contributing to the increased CH_4 conversion. In addition, when Mn^{3+} reacts with CH_4, it can produce a methyl radical, which explains why 33Mn15Ca/Ce has higher C_2 selectivity than the 33Mn/Ce catalyst. Furthermore, as shown in Table 2, the 33Mn15Ca/Ce catalyst has a larger $(O_2^-+O_2^{2-})/O^{2-}$ ratio than the 33Mn/Ce catalyst, which explains why its catalytic activity is superior to that of the 33Mn/Ce catalyst.

3.3. 2. Gas composition

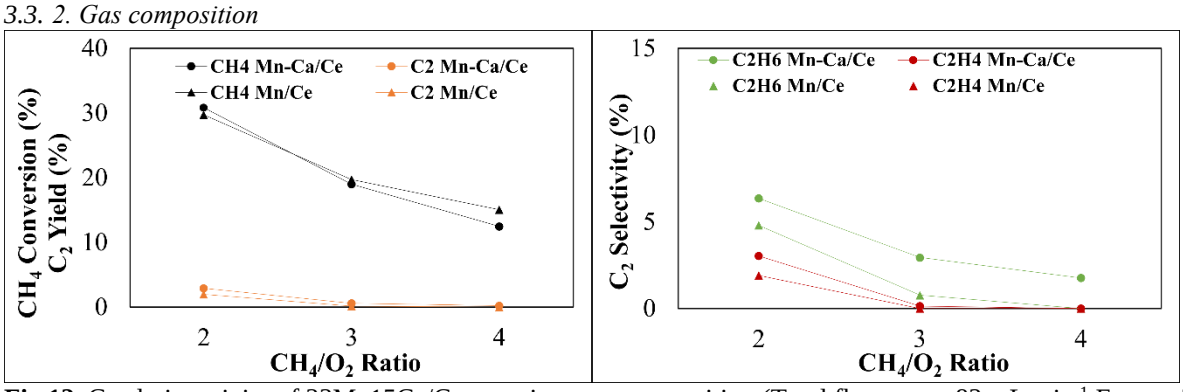

Fig.12. Catalytic activity of 33Mn15Ca/Ce at various gas composition (Total flow rate = 83 mL min^{-1};$F_{(CH4)}$ = 55 mL min^{-1};He balance, temperature = 450 ºC, catalyst weight = 60 mg, W/F = 0.3 g h mol^{-1})

Another observation is carried out to acquire a better understanding of the 33Mn15Ca/Ce performance. The reaction was carried out at 450 ºC with varying CH_4/O_2 ratios. The feed contains CH_4 and O_2, with a CH_4/O_2 ratio of 2. Furthermore, Helium (He) is introduced to the gas composition as an inert balance gas at CH_4/O_2 ratios of 3 and 4. As shown in Fig. 12, both catalysts experience a drop in CH_4 conversion and C_2 yield when the CH_4/O_2 ratio increases. The increase in the CH_4/O_2 ratio shows a drop in oxygen partial pressure, implying that fewer oxygen molecules are adsorbed on the catalyst surface. Furthermore, 33Mn15Ca catalyst has lower methane conversion than 33Mn catalyst when the methane to oxygen ratio increases. Raman spectroscopy result shows that the 33Mn15Ca/Ce catalyst has fewer oxygen vacancies than the 33Mn/Ce catalyst. oxygen vacancy is crucial because it can regenerate active oxygen species. As a result, in oxygen-leaning conditions, where there is only a small quantity of oxygen vacancy, the regeneration of active oxygen species is substantially slower, resulting in lower CH_4 conversion over 33Mn15Ca/Ce catalyst.

Interestingly, even though the methane conversion of 33Mn15Ca/Ce catalyst is lower than 33Mn/Ce catalyst at low oxygen partial pressure, the C_2 yield of 33Mn15Ca/Ce catalyst remained higher than 33Mn/Ce catalyst. The selectivity of both catalysts decreases as the lower oxygen partial pressure is applied. 33Mn15Ca/Ce catalyst surprisingly gives better result than 33Mn catalyst in terms of product selectivity. It indicates that although 33Mn15Ca has fewer amount of oxygen vacancies, its ability in turning methane into methyl radicals is compensated by the superoxide and peroxide anions that exist in 33Mn15Ca catalyst surface, based on Raman spectroscopy result. Therefore, it can produce more ethane and ethylene even at low oxygen pressure conditions.

3.3. 3. Contact time

Contact time affects both the 33Mn/Ce and 33Mn15Ca/Ce catalysts. The catalyst was tested at 450 ºC in a CH_4/O_2 ratio of 3, with varied catalyst weights representing W/F values of 0.15, 0.3, and 0.6 g hr mol^{-1}. The increase in W/F indicates a longer contact time condition. As demonstrated in Fig. 13, both catalysts exhibit a small increase in W/F CH_4 conversion and C_2 production during longer contact times. Furthermore, the 33Mn/Ce catalyst exhibits a decrease in C_2 yield with longer contact time. On the contrary, 33Mn15Ca/Ce improves C_2 yield with longer contact times.

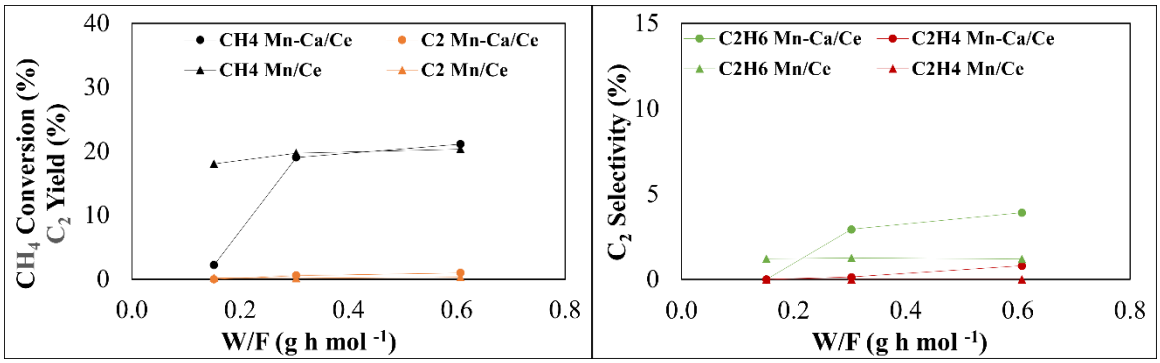

Fig.13. Catalytic activity of 33Mn15Ca/Ce at various contact time (CH_4/O_2 ratio in 3, total flow rate = 83 mL min^{-1};$F_{(CH4)}$ = 55 mL min^{-1};He balance, temperature = 450 ºC, catalyst)

This phenomenon may arise because longer contact time conditions are advantageous for the 33Mn15Ca/Ce. A longer contact time benefits catalysts with lower levels of oxygen vacancy in regenerating active oxygen species. It lets the O_2 stay a little longer in the vacant oxygen space to regenerate active oxygen species. Thus, this condition has a positive impact on C_2 formation. However, for the 33Mn/Ce catalyst, a longer contact time is detrimental to the OCM reaction because the generated C_2 may be further oxidized to produce CO_2, resulting in a drop in C_2 yield. The presence of O^{2-} on the catalyst surface can cause further oxidation.

According to the XRD data, MnO_2, which contains an O^{2-} anion, is formed on the 33Mn/Ce. On the other hand, $CaMn_3O_6$ is detected, which has the advantage of lowering the amount of O^{2-} on the catalyst surface, hence suppressing further oxidation of C_2 products. As a result, the 33Mn15Ca/Ce catalyst transforms more CH_4 and produces more C_2H_6 and C_2H_4 over a longer contact time than the 33Mn/Ce catalyst.

IV. Conclusion

In this study, to develop catalysts that have the potential for methane oxidative coupling, a series of 33MnX/Ce catalysts with different X metals (X = Ca, La, Li, and Zr) were synthesized and studied using various approaches.

1) Adding Ca to 33Mn/Ce catalyst improves catalytic performance at 450 ºC.
2) XRD examination showed the formation of MnO_2 and $CaMn_3O_6$ perovskite over 33Mn/Ce and 33Mn15Ca catalysts, respectively. Raman study revealed that the addition of Ca to 33Mn/Ce catalyst lowers the number of oxygen vacancies. In addition, the formation of the O_2^{2-} anion was observed. N_2 adsorption-desorption experiments demonstrated that the 33Mn15Ca/Ce catalyst had a lower surface area and a larger pore size than the 33Mn/Ce catalyst. XPS data show that the 33Mn15Ca/Ce catalyst has fewer Ce^{3+} cations, more surface electrophilic oxygen, and more Mn^{3+} cations than the 33Mn/Ce catalyst.
3) Additional observations of 33Mn15Ca/Ce catalytic performance were examined. Various reaction temperatures, gas compositions, and contact times were tested. The 33Mn/Ce catalyst performs better at 400 ºC due to its abundance of Ce^{3+} and oxygen vacancies. When heated to 450 ºC, 33Mn15Ca/Ce performs better due to its abundance of surface electrophilic oxygen. Furthermore, the increase in Mn^{3+} quantity caused by Ca addition influences the rise in catalytic activity. At oxygen-leaning conditions, the 33Mn/Ce catalyst performs better than the 33Mn15Ca/Ce. This can happen because the 33Mn/Ce catalyst has more oxygen vacancies than the 33Mn15Ca/Ce catalyst. At longer contact times, the 33Mn15Ca/Ce catalyst performs better than the 33Mn/Ce catalyst. $CaMn_3O_6$ perovskite that exists on the 33Mn15Ca/Ce catalyst is believed to limit the further oxidation of C_2 products.

Therefore, it is discovered that adding calcium can boost the yield of C_2 products by increasing the concentration of Mn^{3+} cation and surface electrophilic oxygen on the catalyst surface. Mn^{3+} cation is beneficial in getting more surface electrophilic oxygen production over the catalyst surface, which is favorable for C_2 product generation.

Acknowledgements

Part of this research was supported by JST CREST (JPMJCR16P3).

REFERENCES

[1]. M Ozaki, Y. Adachi, Y. Iwahori, and N. Ishii, Application of fuzzy theory to writer recognition of Chinese characters, International Journal of Modelling and Simulation, 18(2), 1998, 112-116.
[2]. Global Greenhouse Gas Emissions Data | US EPA. (2024, February 7). US EPA. https://www.epa.gov/ghgemissions/global-greenhouse-gas-emissions-data

[3]. Wang D, Rosynek MP, Lunsford JH, Oxidative Coupling of Methane over Oxide-Supported Sodium-Manganese Catalysts, Journal of Catalysis, 155(2), 1995, 390-402.

[4]. Maulidanti EG, Awaji M, Asami K, Low temperature oxidative coupling of methane over cerium oxide based catalyst. Gas Science and Engineering, 116(20505)7, 2023.

[5]. Huang, Z., Xi, S., Song, J., Dou, S., Li, X., Du, Y., Diao, C., Xu, Z. J., & Wang, X, Tuning of lattice oxygen reactivity and scaling relation to construct better oxygen evolution electrocatalyst. Nature Communications, 12(1), 2021.

[6]. Zhang, H., Gu, J., Tong, J., Hu, Y., Guan, B., Hu, B., Zhao, J., & Wang, C, Hierarchical porous MnO_2 /CeO_2 with high performance for supercapacitor electrodes. Chemical Engineering Journal, 286, 2016, 139–149.

[7]. Li, S., Zheng, Z., Zhao, Z., Wang, Y., Yao, Y., Liu, Y., Zhang, J., & Zhang, Z, CeO_2 Nanoparticle-Loaded MnO_2 Nanoflowers for Selective Catalytic Reduction of NOx with NH3 at Low Temperatures. Molecules/Molecules Online/Molecules Annual, 27(15), 2022, 4863.

[8]. Wang, Y., Xie, Y., Sun, H., Xiao, J., Cao, H., & Wang, S, Hierarchical shape-controlled mixed-valence calcium manganites for catalytic ozonation of aqueous phenolic compounds. Catalysis Science & Technology, 6(9), 2016, 2918–2929.

[9]. Cui, Y., Xu, L., Zhang, Y., Wu, C., Zou, W., Zhang, L., Wang, N., Dong, L., & Chen, M, Oxidation of Toluene over Mesoporous MnO_2/CeO_2 Nanosphere Catalysts: Effects of the MnO_2 Precursor and the Type of Support. Inorganic Chemistry, 62(25), 2023, 9983–10002.

[10]. Reddy, B. M., Khan, A., Yamada, Y., Kobayashi, T., Loridant, S., & Volta, J, Raman and X-ray Photoelectron spectroscopy study of CeO_2−ZrO_2 and V_2O_5/CeO_2−ZrO_2 catalysts. Langmuir, 19(7), 2003, 3025–3030.

[11]. Kainbayev, N., Sriubas, M., Virbukas, D., Rutkuniene, Z., Bockute, K., Bolegenova, S., & Laukaitis, G, Raman Study of Nanocrystalline-Doped Ceria Oxide Thin Films. Coatings, 10(5), 2020, 432.

[12]. Matsushita, I., Suzuki, T., Moriga, T., Ashida, T., Nakabayashi, I., & Metson, J, XPS Study on the Carbonation Process of Ca(OH)₂ Nihon Seramikkusu Kyoukai Gakujyutsu Rombunshi/Nippon Seramikkusu Kyōkai Gakujutsu Rombunshi, 101(1174), 1993, 725–727.

[13]. Hu, Z., Liu, X., Meng, D., Guo, Y., Guo, Y., & Lu, G, Effect of Ceria Crystal Plane on the physicochemical and catalytic properties of PD/Ceria for CO and propane oxidation. ACS Catalysis, 6(4), 2016, 2265–2279.

[14]. Zhou, Y., Perket, J. M., & Zhou, J, Growth of PT nanoparticles on reducible CeO_2(111) thin films: effect of nanostructures and redox properties of CERIA. Journal of Physical Chemistry. C./Journal of Physical Chemistry. C, 114(27), 2010, 11853–11860.

[15]. Zhang, Y., Xu, J., Xu, X., Xi, R., Liu, Y., Fang, X., & Wang, X, Tailoring La2Ce2O7 catalysts for low temperature oxidative coupling of methane by optimizing the preparation methods. Catalysis Today, 355, 2020, 518–528.

[16]. Xu, J., Peng, L., Fang, X., Fu, Z., Liu, W., Xu, X., Peng, H., Zheng, R., & Wang, X, Developing reactive catalysts for low temperature oxidative coupling of methane: On the factors deciding the reaction performance of Ln 2 Ce 2 O 7 with different rare earth A sites. Applied Catalysis. A, General, 552, 2018, 117–128.

[17]. Nesbitt, H. W., & Banerjee, D, Interpretation of XPS Mn(2p) spectra of Mn oxyhydroxides and constraints on the mechanism of MnO_2 precipitation. ˜ the œAmerican Mineralogist, 83(3–4),1998, 305–315.

[18]. Ilton, E. S., Post, J. E., Heaney, P. J., Ling, F. T., & Kerisit, S. N, XPS determination of Mn oxidation states in Mn (hydr)oxides. Applied Surface Science, 366, 2016, 475–485.

[19]. Asami, K., Fujita, T., Nishiyama, Y., & Ohtsuka, Y, Formation of Ethane and Ethylene from Methane and Carbon Dioxide over Manganese Oxide Catalysts. Sekiyu Gakkaishi, 39(2), 1996, 137–143.

[20]. Maulidanti, Ellen Gustiasih and Osaki, Riko and Nakashima, Rui and Asami, Kenji, Catalytic Performance of Mn/CeO_2 Catalyst for Low Temperature Oxidative Coupling of Methane. Available at SSRN: https://ssrn.com/abstract=4707104

[21]. Huang, J., Huang, H., Liu, L., & Jiang, H, Revisit the effect of manganese oxidation state on activity in low-temperature NO-SCR. Molecular Catalysis, 446, 2018, 49–57.